Finite-temperature full random-phase approximation model of band gap narrowing for silicon device simulation

Andreas Schenk[a)]
Swiss Federal Institute of Technology, Integrated Systems Laboratory, Gloriastrasse 35, CH-8092 Zürich, Switzerland

(Received 22 January 1998; accepted for publication 1 July 1998)

An analytical model of the band gap narrowing (BGN) in silicon was derived from a non-self-consistent finite-temperature full random-phase approximation (RPA) formalism. Exchange-correlation self-energy of the free carriers and correlation energy of the carrier-dopant interaction were treated on an equal basis. The dispersive quasi-particle shift (QPS) in RPA quality was numerically calculated for a broad range of densities and temperatures. The dispersion was found to be smooth enough for the relevant energies to justify the rigid shift approximation in accordance with the non-self-consistent scheme. A pronounced temperature effect of the BGN only exists in the intermediate density range. The contribution of the ionic part of the QPS to the total BGN decreases from 1/3 at low densities to about 1/4 at very high densities. Based on the numerical results, Padé approximations in terms of carrier densities, doping, and temperature with an accuracy of 1 meV were constructed using limiting cases. The analytical expression for the ionic part had to be modified for device application to account for depletion zones. The model shows a reasonable agreement with certain photoluminescence data and good agreement with recently revised electrical measurements, in particular for p-type silicon. The change of BGN profiles in a bipolar transistor under increasing carrier injection is demonstrated. © *1998 American Institute of Physics.* [S0021-8979(98)06519-0]

I. INTRODUCTION

Heavy doping of certain regions in semiconductor devices and/or large carrier concentrations due to optical excitation or high electrical injection both result in a shrinkage of the band gap. For the first case, the term ''doping-induced band gap narrowing (BGN)'' came into use, in the second case people often refer to ''plasma-induced BGN.'' As a consequence of BGN, the effective intrinsic density can increase by orders of magnitude. BGN has a strong impact on device operation, in particular on the current gain of bipolar transistors as shown in Fig. 1. Since in a bipolar transistor the plasma-induced BGN is very nonuniform both across the emitter-base junction and throughout the base, it affects the barrier for minority carriers in the junction and also the effective drift field in the base. In Fig. 1 we compared common empirical BGN models either based on ''apparent'' BGN data, i.e., on electrical measurements of the pn product in bipolar transistors (''Slotboom,'' [1–3] ''del Alamo'' [4–6]) or on absorption data (''Bennett/Wilson'' [7]) with room-temperature photoluminescence (PL) measurements by Wagner.[8–10] The simulated current gains of an npn transistor with a peak emitter concentration of about 10^{20} cm^{-3} differ largely when using one of these models, despite the fact that all models predict a quite similar ΔE_g for this particular density. The overestimation of the gain increases with the underestimation of the BGN in the emitter, since the former is proportional to $n_{\text{base}}/p_{em} \sim \exp(-\Delta E_g/k_B T)$.[11] High injection levels giving rise to plasma-induced BGN also occur in photoconductive switches, concentrator solar cells, and power devices operated in the on-state.

In case of a neutral plasma we may distinguish between two situations: a symmetrical electron-hole (e-h) plasma (e.g., by laser excitation of intrinsic material) and a asymmetrical e-h plasma (e.g., by laser excitation of doped material, or more importantly, the heavily doped, neutral regions of electronic devices). In the second case, charge balance involves electrically active dopants. Neugroschel *et al.*[12] found evidence for e-h plasma densities up to 4×10^{18} cm^{-3} in low-doped collector regions of silicon bipolar transistors subjected to strong electrical excitation. In interpreting their data they assumed an additional BGN of up to 80 meV caused by the plasma. Banghart and Gray[13] pointed out that the effective recombination lifetime extracted from open-circuit voltage decay data can be largely reduced due to plasma-induced BGN. They fitted theoretical results of Lowney[14] by the expression $\Delta E_{g,\text{e-h}} = \alpha n^{\beta}$ where $\alpha = 3.83\times10^{-7}$ meV cm$^{3\beta}$ and $\beta = 0.438$ for densities n between 5×10^{16} and 8×10^{17} cm^{-3}, and $\alpha = 2.90\times10^{-5}$ meV cm$^{3\beta}$ and $\beta = 0.333$ for densities n between 8×10^{17} and 1×10^{19} cm^{-3}. Another fit to the results of Lowney was given by Shaheed and Maziar:[15] $\Delta E_{g,\text{e-h}} = 3.81\times10^{-6} n^{0.38}$ meV with the plasma density n in cm^{-3}.

To avoid confusion with the term ''doping-induced BGN'' when the plasma originates from a doped region, we should point out that doping serves, first of all, as the source of free carriers, i.e., as the source of plasma-induced BGN, and secondarily it causes an additional BGN contribution by the carrier-dopant interaction. The latter is very sensitive to

[a)]Electronic mail: schenk@iis.ee.ethz.ch

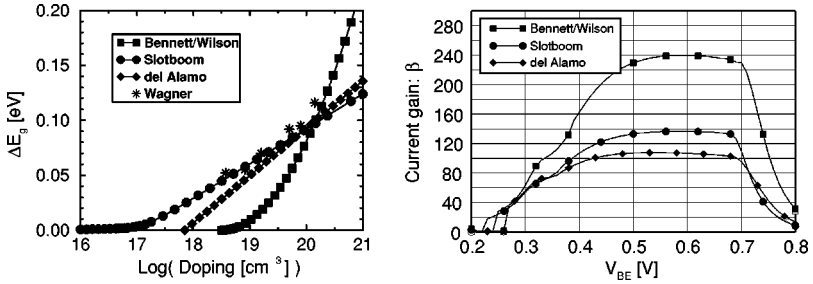

FIG. 1. Empirical BGN models (left) in comparison with room-temperature photoluminescence data (stars) and the corresponding current gain simulations of a bipolar transistor (right).

the density of the present asymmetrical plasma, which screens the carrier-dopant interaction. Obviously, it is more transparent to distinguish between the following two BGN contributions: the exchange-correlation energy of the carrier–carrier interaction, and the correlation energy of the carrier-dopant interaction. In this article both contributions will be treated on the same theoretical basis.

Earlier theoretical approaches to BGN were mostly restricted to the $T=0$ limit. Mahan[16] performed a Hartree-Fock variational calculation of the ground state energy of the electron-donor system in n-type silicon valid up to concentrations of 10^{20} cm^{-3} neglecting band tailing and assuming that the donors are distributed on a regular *fcc* sublattice. The hole and electron correlation energies were taken into account in the single plasmon pole (SPP) approximation.[17] Berggren and Sernelius[18] derived the self-energy of the electron-donor interaction from second-order perturbation theory for a *random* system of impurities. They included a random-phase approximation (RPA) dielectric screening in their $T=0$ calculation. The different treatment of the arrangement of dopants resulted in a large difference of the corresponding electron-ion self-energy contributions at high densities. Berggren and Sernelius[19] found that the model of complete disorder produces a large shift even *without* the inclusion of multivalley scattering in contrast to Selloni and Pantelides,[20,21] who obtained a negligible effect if multivalley scattering is omitted. Abram *et al.*[22] calculated the plasma-induced zero-temperature quasi-particle shift (QPS) at the band extrema of n- and p-type silicon using the SPP approximation including a q^4 term in the plasmon dispersion relation, which brings the accuracy close to that of the Lindhard dielectric function.[23] Logan and Egley[24] obtained the QPS for highly doped p-type silicon using band dispersions based on a 6×6 Hamiltonian and approximate self-energies in a finite-temperature dielectric-response formalism: a statically screened Hartree-Fock exchange potential (which neglects dynamic screening and the ''Coulomb hole term,'' i.e., the correlation part of the QPS) and the second-order perturbation term of electron-impurity interaction ($T=0$). Their results agreed quantitatively with the PL data by Wagner for p-type silicon[8,10] both at 20 and 300 K. An accurate RPA expression for the QPS in a symmetrical e-h plasma valid at all temperatures, was derived by Zimmermann.[25] The asymmetrical case (extrinsic semiconductor with plasma excitation) had been worked out by Rösler *et al.*[26] They considered the ions as dynamic quantities with infinite mass assuming complete disorder. Their numerical results based on RPA were given for $T=0$ K only.

In this article we will follow the theoretical framework of Zimmermann and co-workers.[25–29] The very goal is to derive a BGN model for silicon device simulation based on the most sound theory which is capable to meet this goal. Therefore, the non-self-consistent full RPA at finite temperatures is applied to both the exchange-correlation self-energy of the free carriers and the correlation energy of the carrier-dopant interaction. Numerical results for the rigid band shifts are then used to fit analytical expressions of the BGN as function of carrier densities, doping, and temperature. The dispersive QPS is also calculated for a variety of densities and temperatures, but is not translated into a BGN model because of the consistency between rigid shift approximation and non-self-consistent RPA.

The article is organized as follows: Section II gives a brief outline of the theory and presents numerical RPA results. Analytical fits for the rigid QPS in homogeneous systems are derived in Sec. III. In Sec. IV the BGN formulas are modified for device simulation and compared against experimental data there. We demonstrate the variation of the BGN profile in a bipolar transistor under different injection conditions. Finally, conclusions are given in Sec. V.

II. BASIC THEORY AND NUMERICAL RESULTS

In the electron-hole picture, with the reference state being the Hartree-Fock bands of the intrinsic, nonexcited crystal at zero temperature, we restrict ourselves to the model of parabolic bands $E_a^0(k)=\hbar^2k^2/2m_a$ ($a=e$ for electrons, $a=h$ for holes). The multivalley conduction band, heavy and light hole bands, and spin summation are condensed in degeneracy factors g_a ($g_e=12$ for electrons, $g_h=4$ for holes). The effective masses m_a are understood as density of states (DOS) effective masses ($m_e=(m_t^2m_l)^{1/3}$ for electrons, $m_h=[(m_{\mathrm{lh}}^{3/2}+m_{\mathrm{hh}}^{3/2})/2]^{2/3}$ for holes). Silicon parameters used in the calculation are listed in Table I, where μ^* is the reduced effective mass, ϵ_s the static dielectric constant, $\mathrm{Ry}_{\mathrm{ex}}$ the excitonic Rydberg, a_{ex} the excitonic Bohr radius, and $\alpha_a=\mu^*/m_a$. On the same level of approximation, Bloch states in the intraband Coulomb matrix elements can be approximately treated as plane waves. The crude band model is justified by the experience that the sum of exchange and correlation energy depends rather weakly on band-structure details as valley degeneracy, mass anisotropy, and valence

TABLE I. Silicon parameters used in the calculation.

m_e/m_0	m_h/m_0	g_e	g_h	μ^*/m_0	α_e	α_h	$\mathrm{Ry}_{\mathrm{ex}}$	a_{ex}	ϵ_s
0.321	0.346	12	4	0.1665	0.5187	0.4813	16.55 meV	37.19×10^{-8} cm	11.7

band coupling, mainly due to a compensation effect. This was proven by RPA[25] and fully self-consistent calculations.[30]

The quasi-particle shift (QPS) $\Delta_a(k)$ is introduced as difference between free and interacting dispersion[25] (to simplify the notation the vector character of momenta and coordinates is not written explicitly, and the normalization volume V_0 is set to unity):

$$E_a(k)=\hbar^2k^2/2m_a+\Delta_a(k), \tag{1}$$

where $\Delta_a(k)$ is given by the real part of the self-energy at ''frequency'' $E_a(k)+i0^+$,

$$\Delta_a(k)=\mathrm{Re}\,\Sigma_a[k,E_a(k)+i0^+]. \tag{2}$$

Obviously, Eq. (1) defines a self-consistent problem because the quasi-particle energy $E_a(k)$ enters the QPS. A self-consistent RPA calculation at finite temperatures is outside the range of practicability. A test calculation for one particular density, zero temperature, using the SPP approximation, and including QP broadening by a complex QP energy was presented by Zimmermann.[25] The main findings were a slight flattening of the QPS dispersion from zero wave vector up to plasmon threshold with an almost unchanged value at the Fermi momentum k_{Fa} and the disappearance of the sharp spike defining the threshold for plasmon emission at $T=0$ K. Therefore, dispersion effects are of minor importance for energies below plasmon threshold, and the dispersive QPS may be replaced by a rigid shift Δ_a. This essentially facilitates BGN modeling. However, instead of using $\Delta_a(0)$, the rigid shift is better fixed by the requirement that the QPS density should not change in first order with respect to $\Delta_a(k)-\Delta_a$. The result is[25]

$$\Delta_a=\frac{\Sigma_k\partial f_a(k)/\partial\zeta_a\ \mathrm{Re}\,\Sigma_a[k,E_a(k)+i0^+]}{\Sigma_k\partial f_a(k)/\partial\zeta_a} \tag{3}$$

with rigidly shifted bands $E_a(k)=\hbar^2k^2/2m_a+\Delta_a$ and Fermi functions $f_a(k)$ depending on shifted chemical potentials μ_a:

$$f_a(k)=f(\hbar^2k^2/2m_a-\zeta_a),\quad \zeta_a=\mu_a-\Delta_a. \tag{4}$$

The QP density in the rigid shift approximation is given by

$$n_a=\sum_k g_a f_a(k)=g_a\Lambda_a^{-3}F_{1/2}(\beta\zeta_a) \tag{5}$$

with the Fermi integral $F_{1/2}$, the thermal wavelength $\Lambda_a=(2\pi\hbar^2\beta/m_a)^{1/2}$, and $\beta=1/k_BT$.

The RPA self-energy at Matsubara frequencies z_a is a convolution of screened potential and one-particle Green's function (''$w\cdot G$-approximation'')

$$\Sigma_a(k,z_a)=-\frac{1}{\beta}\sum_{q\nu} w(q,\Omega_\nu)G_a(k+q,z_a+\Omega_\nu), \tag{6}$$

where

$$\hbar z_a=\frac{i\pi}{\beta}(2n+1)+\mu_a,\quad n\ \text{integer}, \tag{7}$$

$$\hbar\Omega_\nu=\frac{i\pi}{\beta}2\nu,\quad \nu\ \text{integer}. \tag{8}$$

For the one-particle Green's function G_a, the QP form is used:

$$G_a(k,z_a)=G_a^{\mathrm{QP}}(k,z_a)=\frac{1}{\hbar z_a-E_a(k)}. \tag{9}$$

$w(q,\Omega_\nu)$ is the totally screened potential

$$w(q,\Omega_\nu)=\epsilon^{-1}(q,\Omega_\nu)v(q) \tag{10}$$

with the bare potential $v(q)=e^2/(\epsilon_0\epsilon_s q^2)$. The inverse dielectric function can be shown to factorize into an electronic part $\epsilon_{\mathrm{eh}}^{-1}$ and an ionic part ϵ_i^{-1}:

$$\epsilon^{-1}(q,\Omega_\nu)=\epsilon_{\mathrm{eh}}^{-1}(q,\Omega_\nu)\epsilon_i^{-1}(q,\Omega_\nu). \tag{11}$$

Screening by the electron-hole system is described with the RPA dielectric function

$$\epsilon_{\mathrm{eh}}(q,\Omega_\nu)=1-v(q)\sum_{a,k} g_a\frac{f_a(k+q)-f_a(k)}{E_a(k+q)-E_a(k)-\hbar\Omega_\nu}, \tag{12}$$

which gives the electronically screened potential V_s:

$$V_s(q,\Omega_\nu)=\epsilon_{\mathrm{eh}}^{-1}(q,\Omega_\nu)v(q). \tag{13}$$

The ionic part of the inverse dielectric function is related to the position correlation function of the ionic distribution $g_i(r_1,r_2)$. We assume a random arrangement on regular lattice sites R_j, which is considered the most realistic case for a device model:

$$g_i(r_1,r_2)=\left(\frac{N_i}{N}\right)^2\sum_{j\neq l}\delta(r_1-R_j)\delta(r_2-R_l)+\frac{N_i}{N}\left(1-\frac{N_i}{N}\right)\sum_l\delta(r_1-R_l)\delta(r_1-r_2). \tag{14}$$

Here, N_i denotes the number of dopants and N the number of lattice sites in the normalization volume. Using Eq. (14), the ionic part of the inverse dielectric function takes the form

$$\epsilon_i^{-1}(q,\Omega_\nu)=1-\beta V_s(q,0)\delta_{\nu,0}N_i\left(1-\frac{2N_i}{N}\right)\approx1-\beta V_s(q,0)\delta_{\nu,0}N_i, \tag{15}$$

since $N_i\ll N$ holds up to the highest doping densities. Inserting $w(q,\Omega_\nu)$ into Σ_a, the RPA self-energy decays into an electronic part and an ionic part:

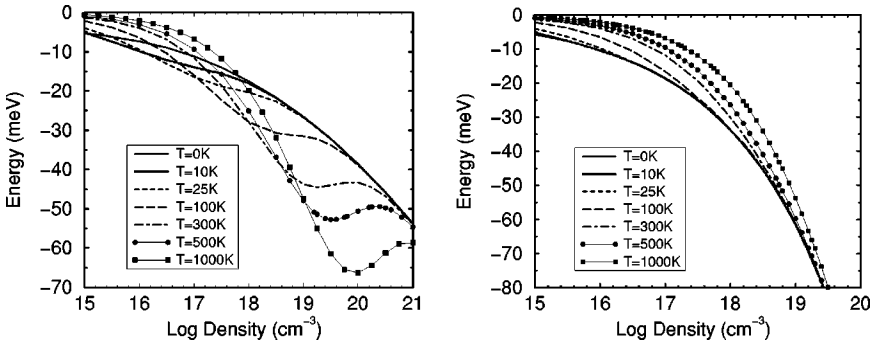

FIG. 2. Correlation part of the average QPS $\Delta_e^c+\Delta_h^c$ (left) and total average QPS $\Delta_e^{xc}+\Delta_h^{xc}$ (right) for a symmetrical e-h plasma as function of plasma density and temperature.

$$\Sigma_a(k,z_a)=\Sigma_a^{xc}(k,z_a)+\Sigma_a^i(k,z_a) \tag{16}$$

with

$$\Sigma_a^{xc}(k,z_a)=-\frac{1}{\beta}\sum_{q,\nu} V_s(q,\Omega_\nu)G_a^{\mathrm{QP}}(k+q,z_a+\Omega_\nu), \tag{17}$$

$$\Sigma_a^i(k,z_a)=N_i\sum_q V_s^2(q,0)G_a^{\mathrm{QP}}(k+q,z_a). \tag{18}$$

The total (dispersive) QPS then is obtained by

$$\Delta_a(k)=\mathrm{Re}\,\Sigma_a^{xc}[k,E_a(k)+i0^+]+\mathrm{Re}\,\Sigma_a^i[k,E_a(k)+i0^+]. \tag{19}$$

However, Matsubara sums or integrations over energy variables in the self-energy have to be performed *prior* to any symbolic substitution $z_a=i\pi/\beta(2n+1)+\mu_a\rightarrow z\in\mathrm{C}$. The numerical evaluation of the formulas is based on the following representation (Ref. 25, p. 53), where an *unscreened* exchange term is extracted from Σ_a^{xc}:

$$\Delta_a(k)=\Delta_a^x(k)+\Delta_a^c(k)+\Delta_a^i(k), \tag{20}$$

with

$$\Delta_a^x(k)=-\int \frac{d^3q}{(2\pi)^3}v(q)f_a(k+q), \tag{21}$$

$$\Delta_a^c(k)=-\mathrm{Re}\int \frac{d^3q}{(2\pi)^3}\{V_s[q,E_a(k+q)-E_a(k)-i0^+]-v(q)\}\times\{f_a(k+q)+f_B[E_a(k+q)-E_a(k)-i0^+]\}-\frac{1}{\beta}\mathrm{Re}\int \frac{d^3q}{(2\pi)^3}\sum_\nu \frac{[V_s(q,\Omega_\nu)-v(q)]}{\hbar\Omega_\nu+E_a(k)-E_a(k+q)+i0^+}, \tag{22}$$

$$\Delta_a^i(k)=-n_i\mathrm{Re}\int \frac{d^3q}{(2\pi)^3}\frac{V_s^2(q,0)}{E_a(k+q)-E_a(k)+i0^+}. \tag{23}$$

Here, $n_i=N_i/V_0$ denotes the impurity concentration (doping) and $f_B(E)=1/[\exp(\beta E)-1]$ the Bose distribution. These equations have to be understood as first iteration of the self-consistent problem, i.e., the QP energy in the r.h.s. must be replaced by the dispersion of the noninteracting carriers.

Inspection of $\Delta_a^c(k)$, $\Delta_a^i(k)$, and the RPA dielectric function ϵ_{eh} shows that in the rigid shift approximation the QPS cancels in all energy differences $E_a(k+q)-E_a(k)$ and that only the Fermi functions depend on it via the Fermi energy $\zeta_a=\mu_a-\Delta_a$, which, however, is directly related to the density n_a. Hence, there is no self-consistency problem in the rigid shift approximation as already mentioned above.

Inserting $\Delta_a(k)$ into the definition of the average rigid shift (3) one obtains[25,26]

$$\Delta_a^x=-\frac{e^2}{4\pi\epsilon_0\epsilon_s\Lambda_a}F_{-1/2}(\beta\zeta_a), \tag{24}$$

$$\Delta_a^c=\frac{1}{2\beta}\int \frac{d^3q}{(2\pi)^3}\sum_\nu [\epsilon_{\mathrm{eh}}^{-1}(q,\Omega_\nu)-1]\frac{\partial\epsilon_{\mathrm{eh}}(q,\Omega_\nu)}{\partial n_a}, \tag{25}$$

$$\Delta_a^i=-\frac{n_i}{2}\left(\frac{\partial n_a}{\partial\zeta_a}\right)^{-1}\int \frac{d^3q}{(2\pi)^3}\frac{v(q)}{\epsilon_{\mathrm{eh}}^2(q,0)}\frac{\partial\epsilon_{\mathrm{eh}}(q,0)}{\partial\zeta_a}. \tag{26}$$

These formulas were evaluated numerically in the density range 10^{15}–10^{21} cm^{-3} and for temperatures between 0 and 1000 K. Some results are plotted in Figs. 2 and 3.

As shown in Fig. 2 the temperature dependence of the average rigid shift Δ^{xc} is only pronounced in the intermediate doping range. This is due to the fact that an almost com-

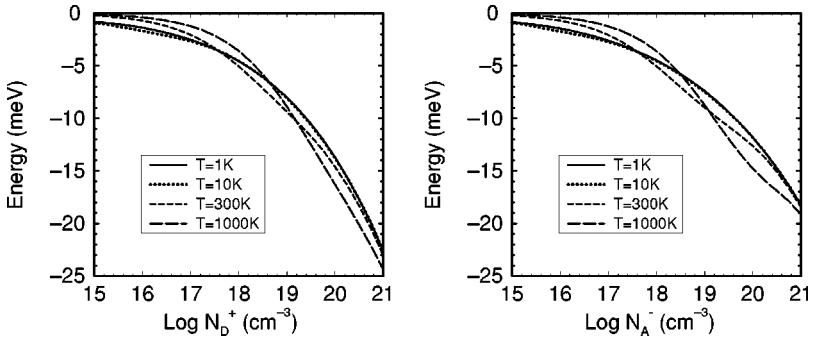

FIG. 3. Ionic part Δ_e^i (left) and Δ_h^i (right) of the average QPS for neutral n- and p-type silicon as function of activated doping concentration and temperature.

plete compensation of the temperature effects in Δ^x and Δ^c takes place.[28] In the high density range all curves merge with the zero-temperature result. At room temperature, the $T=0$ limit becomes exact above 10^{19} cm^{-3}. This may justify the frequent restriction to the $T=0$ limit in the literature, which suffices as long as only the heavy doping range matters. However, around the Mott density the temperature dependence cannot be neglected. If the carriers are not thermalized with the lattice, the question arises, what temperature should be assigned to electrons and holes, respectively. For a *symmetrical* e-h plasma, this question is difficult to answer, since the e-h interaction has a share in establishing quasi-equilibrium.[25] Fortunately, in electronic devices the presence of an e-h plasma caused by high injection goes along with relatively weak internal fields. Thus, carrier heating is mainly a consequence of Joule heating, and the deviation of the carrier temperature from lattice temperature is small. Hence, identification of T with the respective carrier temperature (T_e or T_h) seems to be a practicable way for energy balance and hydrodynamic simulators.

Figure 3 shows the ionic part of the average QPS Δ_e^i (left) and Δ_h^i (right) for neutral n- and p-type silicon, respectively, as function of the activated doping concentration and temperature. It is worth noting that strong screening makes Δ_a^i negligibly small under conditions of high injection.

The first iteration of the electronic part of the *dispersive* QPS $\Delta_e^{xc}(k)$ in RPA quality [Eqs. (21) and (22)] as function of the normalized wave number ka_{ex} is presented in Fig. 4. A similar picture is obtained for the hole part $\Delta_h^{xc}(k)$. These curves required computation times of the order of CPU weeks on most advanced work stations, indicating that self-consistent RPA calculations are still beyond the computational means. The striking feature at zero temperature is the sharp downward spike located approximately at a wave number defined by the threshold for plasmon emission:[25] $E_e(k)=E_e(k_{Fe})+\hbar\omega_p$ ($\hbar\omega_p$ is the plasmon energy). This spike is rapidly washed out as the temperature rises. Above this threshold, the self-energy becomes complex and using a real QP energy resulted in regular substructures at temperatures below 10 K. For Fig. 4, these substructures were smoothed out as it happens when QP broadening is included in a more realistic calculation.[25] Figure 4 proves the above stated weak dispersion of $\Delta^{xc}(k)$ for the *entire* $n-T$ plane in the relevant energy range [$E(k_{Fa})<\hbar\omega_p$ holds for all densities]. Again, this is caused by a considerable compensation of the rather strong individual dispersions of exchange part $\Delta^x(k)$ and correlation part $\Delta^c(k)$, respectively.[31]

III. FIT FORMULAS FOR HOMOGENEOUS SYSTEMS

In order to derive an analytical BGN model for device simulation we construct Padé approximations in a similar way as in Refs. 28, 32, and 33. Compared to earlier papers we are faced with two additional problems here: The most frequent case in electronic devices is a strongly asymmetrical plasma (heavily doped neutral regions), which inhibits simple fits of the form $\Delta_a^{xc}\sim-(n_e+n_h)^{1/4}$ proposed in Ref. 31 for the symmetrical plasma. (The exchange energy of the minority carriers is zero in heavily doped regions, which prevents a fit in terms of the sum n_e+n_h.) The second complication for a device model arises from space charge regions, where charge neutrality and screening by free carriers are lost. Below, this problem will be discussed in more detail.

For a fit of Δ_a^{xc}, we use the symmetrical e-h plasma. Approximations have to be based on the knowledge of analytical expressions in limiting cases (high density/low temperature and low density/high temperature). In the case of the low-temperature correlation energy analytical results of the SPP approximation can be quoted. In detail, we have in the low density/high temperature limit:

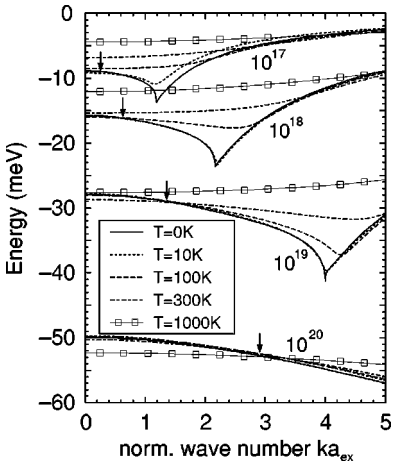

FIG. 4. Dispersive QPS $\Delta_e^{xc}(k)$ as function of normalized wave number ka_{ex} and temperature for various densities of a symmetrical e-h plasma. The arrows indicate the values of the respective Fermi momentum.

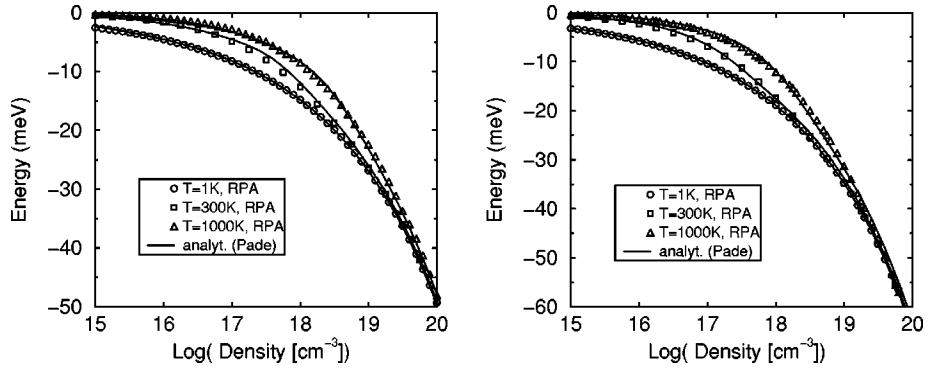

FIG. 5. Average QPS Δ_e^{xc} (left) and Δ_h^{xc} (right) for a symmetrical e-h plasma as function of plasma density and temperature. Comparison between RPA results (symbols) and Padé approximation Eq. (33) (lines).

$$\Delta_a^x(T\to\infty) = -\left(\frac{8\pi\alpha_a}{g_a}\right)\frac{n_a}{\mathscr{T}}, \tag{27}$$

$$\Delta_a^c(T\to\infty) = -\sqrt{\frac{8\pi n_\Sigma}{\mathscr{T}}}\left(1 - b_a\frac{\sqrt{n_\Sigma}}{\mathscr{T}}\right) \approx -\frac{\sqrt{8\pi n_\Sigma/\mathscr{T}}}{1+b_a\sqrt{n_\Sigma}/\mathscr{T}}, \tag{28}$$

with $\mathscr{T}\equiv k_BT/Ry_{\rm ex}$ and $n_\Sigma\equiv n_e+n_h$. In Eq. (28) the first term is the classical Debye shift. Here and in the following equations all densities are normalized by $a_{\rm ex}^{-3}$, and all energies by $\mathrm{Ry}_{\rm ex}$. The parameter b_a will be used to fit the Padé formula for the *sum* of exchange and correlation.

In the high density/low temperature limit the exchange energy is given by

$$\Delta_a^x(T=0) = -\left(\frac{48}{\pi g_a}\right)^{1/3} n_a^{1/3}. \tag{29}$$

For the correlation part $\Delta_a^c(T=0)$, we assume that it depends on the densities via the plasmon energy $\hbar\omega_p = \sqrt{16\pi n_p}$ with $n_p\equiv\alpha_e n_e+\alpha_h n_h$. The SPP result $\Delta_a^c(T=0)\sim-\sqrt{\hbar\omega_p}$ was found to be unacceptable in this range. Instead, we follow Refs. 28, 32, and 33 and use the logarithmic form

$$\Delta_a^c(T=0) = -c_a\,\ln(1+d_a n_p^{p_a}) \tag{30}$$

with fit parameters c_a, d_a, and p_a.

Combination of both limiting cases yields

$$\Delta_a^{xc}(n_e,n_h,T) = \frac{U^{xc}(n_e,n_h,T)\Delta_a^{xc}(0)+\Delta_a^x(\infty)-\sqrt{8\pi n_\Sigma/\mathscr{T}}}{U^{xc}(n_e,n_h,T)+1+b_a\sqrt{n_\Sigma}/\mathscr{T}}, \tag{31}$$

where the function $U^{xc}(n_e,n_h,T)$ switches from the nondegenerate region to strong degeneracy. The relevant expansion parameter would be $\overline{n_a}=n_a\Lambda_a^3/g_a$ for a one-component plasma. Following Ref. 28 a quadratic dependence of U^{xc} on $\overline{n}$ is required. For simplicity of the final formula and based on the best fit with our numerical results, we choose

$$U^{xc}(n_e,n_h,T) = U^{xc}(n_\Sigma,\mathscr{T}) = \left(\frac{4\pi}{\mathscr{T}}\right)^3 n_\Sigma^2. \tag{32}$$

The final Padé approximation of Δ_a^{xc} then reads

$$\Delta_a^{xc}(n_e,n_h,T) = -\frac{(4\pi)^3 n_\Sigma^2\left[\left(\frac{48n_a}{\pi g_a}\right)^{1/3}+c_a\,\ln(1+d_a n_p^{p_a})\right]+\left(\frac{8\pi\alpha_a}{g_a}\right)n_a\mathscr{T}^2+\sqrt{8\pi n_\Sigma}\mathscr{T}^{5/2}}{(4\pi)^3 n_\Sigma^2+\mathscr{T}^3+b_a\sqrt{n_\Sigma}\mathscr{T}^2+40n_\Sigma^{3/2}\mathscr{T}}. \tag{33}$$

The last term in the denominator was introduced in order to improve the fit of the ''swing-over'' in the transition region, where the behavior changes from a $n^{1/2}$ dependence (Debye limit) to an approximate $n^{1/4}$ dependence. This term was found superior to the logarithmic weakening proposed in Ref. 28. Parameters are listed in Table II. In Fig. 5 we compare the Padé approximation for Δ_a^{xc} with the numerical RPA results.

TABLE II. Parameters for Padé approximation Eq. (33).

b_e	b_h	c_e	c_h	d_e	d_h	p_e	p_h
8	1	1.3346	1.2365	0.893	1.153	7/30	7/30

We now proceed with the ionic part Δ_a^i assuming homogeneously doped and uncompensated material. The Debye limit is easily obtained by inserting the Thomas-Fermi approximation of the static dielectric function into Eq. (26):

$$\Delta_a^i(T\to\infty) = -n_i\frac{\sqrt{2\pi}}{\sqrt{\mathscr{T}n_\Sigma}}. \tag{34}$$

Note that this is just one half of $\Delta_a^c(T\to\infty)$, if n_i is replaced

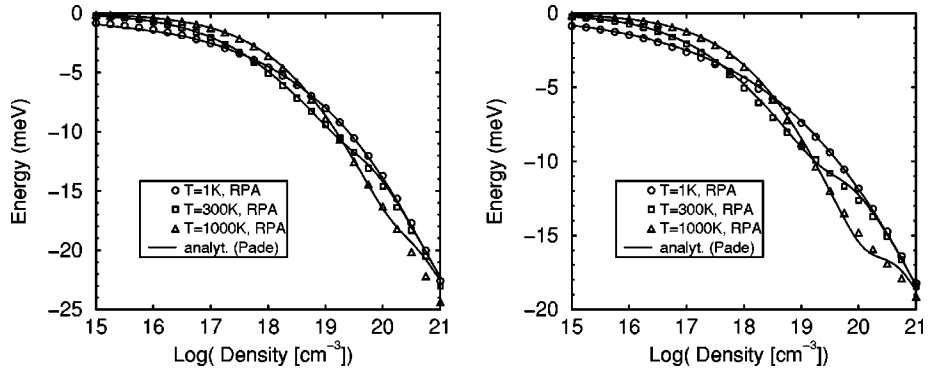

FIG. 6. Ionic QPS part Δ_e^i in neutral n-type silicon (left) and Δ_h^i in neutral p-type silicon (right) as function of density and temperature. Comparison between RPA results (symbols) and Padé approximation Eq. (37) (lines).

by n_Σ. As in the exchange-correlation case [compare Eq. (28)] we add a correction term to extend the validity to higher densities. The form

$$\Delta_a^i(T\to\infty) = -n_i \frac{\sqrt{2\pi}}{\sqrt{\mathscr{T} n_\Sigma}(1+h_a\sqrt{n_\Sigma/\mathscr{T}})} \tag{35}$$

with a fit parameter h_a serves as starting point for the Padé approximant of Δ_a^i. In the high density/low temperature limit we use the special SPP approximation by Thuselt,[31] which gives the analytical result

$$\Delta_a^i(T=0) = -n_i \frac{0.799\alpha_a}{n_p^{3/4}}. \tag{36}$$

Again, the typical $n^{1/4}$ dependence of the correlation energy appears, if n_i is replaced by the carrier density in a doped region. Since the SPP approximation looses accuracy with increasing density, we multiply $n_p^{3/4}$ by a correction term $(1+k_a n_p^{q_a})$ with fit parameters k_a and q_a. Combining both limiting cases yields

$$\Delta_a^i(n_i,n_e,n_h,T) = -\frac{n_i[1+U^i(n_\Sigma,\mathscr{T})]}{\sqrt{\mathscr{T} n_\Sigma/2\pi}[1+h_a\,\ln(1+\sqrt{n_\Sigma/\mathscr{T}})]+j_a U^i(n_\Sigma,\mathscr{T}) n_p^{3/4}(1+k_a n_p^{q_a})}, \tag{37}$$

where the function $U^i(n_\Sigma,\mathscr{T})$ switches from the nondegenerate region to strong degeneracy. Based on the best fit with our numerical results we use

$$U^i(n_\Sigma,\mathscr{T}) = \frac{n_\Sigma^2}{\mathscr{T}^3} \tag{38}$$

here. A logarithmic weakening was introduced in the correction term of the Debye limit. The four parameters h_a, j_a, k_a, and q_a are listed in Table III. In Fig. 6 the Padé approximation for Δ_a^i is compared with the numerical RPA results. The absolute accuracy of the Padé formulas is about 1 meV for both Δ_a^{xc} and Δ_a^i, which is reasonable considering the approximations discussed so far and in the following. In Fig. 7 we demonstrated the relative contribution of the ionic part $\Delta_e^i+\Delta_h^i$ to the total BGN for neutral, uncompensated silicon.

TABLE III. Parameters for Padé approximation Eq. (37).

h_e	h_h	j_e	j_h	k_e	k_h	q_e	q_h
3.91	4.20	2.8585	2.9307	0.012	0.19	3/4	1/4

This contribution decreases from 1/3 at low densities to about 1/4 at extremely high densities. In the Debye limit the ratio is exactly 1/3 as described above.

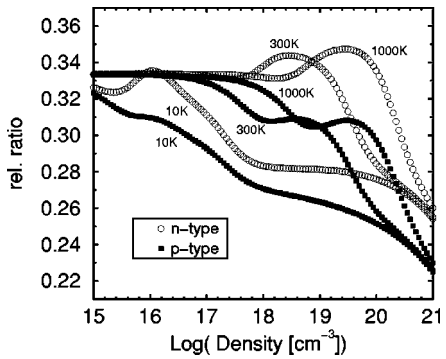

FIG. 7. Relative contribution of the ionic QPS to the total BGN in neutral n-type (circles) and neutral p-type silicon (squares) as function of density and temperature (Padé approximations used).

IV. APPLICATION TO DEVICE SIMULATION

A. Simplifications

In modern devices the doping and carrier concentration profiles may be very steep. The pn-junction of silicon tunnel diodes or the emitter-base junction of modern bipolar transistors have a typical width of 50 nm only (compare Fig. 12). The question arises to which extent the RPA theory of a 3D homogeneous system can be applied to such situations. Zimmermann *et al.*[34] showed that the RPA can be well extended to the calculation of band shifts in quantum wells with a width down to 10 nm. Here, BGN occurs as nondiagonal matrix problem in the confinement functions and strongly depends on the occupation of sublevels. As a general result, the spatial variation of BGN turned out to be less pronounced from a RPA than from a LDA calculation.

Since the correlation radius is approximately given by the screening length, spatial variations in the device should be smooth when compared against the latter. In practice, this condition is often violated. In a metal–oxide–semiconductor field effect transistor (MOSFET) channel the screening length has about the extension of the inversion layer, if the surface concentration is used for the most favorable estimate in a classical calculation. Taking this value to determine the local BGN at the interface would certainly grossly overestimate the effect there. The problem of the locality of the BGN is comparable to all other situations where local quantities are used in device simulation, although a finite volume is necessary for their definition (carrier temperature, effective mass, etc.).

An even more serious problem is caused by the loss of local charge neutrality. Bennett and Lowney[35] noticed that the lack of screening produces a large carrier-impurity contribution to the BGN in depletion regions. Although their theoretical framework[36] is somewhat different from our RPA result Eq. (26), the effect occurs in both approaches and has the same origin: the small value of the free carrier densities in the dielectric screening function. The question arises whether a huge BGN effect can be expected in SCRs. Many-body calculations of the QPS are based on overall charge neutrality. First-order Coulomb terms cancel each other, otherwise, they represent the band bending. Another consequence is the cancellation of the different Hartree terms in the denominator of the QP Green's function Eq. (9). Within a SCR the sum of these terms would become very large making Δ_a^i negligibly small. Hence, the divergent behavior of Δ_a^i given in Eq. (26) appears as simply being due to its inadequate usage in depletion zones. Furthermore, it is clear that the RPA fails for low concentrations even in *neutral* regions of a device. Only if strong screening causes the impurity levels to merge with the band states, i.e., to turn into scattering states, it can yield usable results. In neutral regions, this is the case for densities larger than a few times 10^{18} cm^{-3} (Refs. 37, 38), whereas lower densities, in principle, require a numerical solution of Dyson's equation (Klauder,[39] Serre and Ghazali[40]).

A BGN model for device simulation has to work everywhere in a device, including the SCRs. To overcome the divergency problem we decided for a crude but workable solution. We replace the carrier densities by the respective doping densities in Eq. (37), i.e.,

$$n_\Sigma \to N_D + N_A, \quad n_p \to \alpha_e N_D + \alpha_h N_A, \tag{39}$$

and $n_i \to N_D + N_A$. In neutral and uncompensated regions of a device, the result is the same as from the application of Eq. (37). In SCRs a certain finite rigid shift contribution is artificially produced. Its size is comparable to the band tails that have been studied by many authors ignoring exchange-correlation effects. Approximations leading to Gaussian statistics for the potential fluctuations generally require high doping levels (high-density limit).[41] Van Mieghem *et al.*[42] modeled the effect of band tailing for a noninteracting system as an equivalent downward shift of the Fermi level. In the high-density limit and calculating screening with the unperturbed DOS, an analytical expression was derived, which can be rewritten as $\Delta E_F = -0.62 n_i^{7/24}$ (in units of $\mathrm{Ry_{ex}}$). For silicon, this shift amounts about 15–35 meV in the density range 3×10^{19}–1×10^{21} cm^{-3}.

B. Comparison with experimental data

Both optical and electrical experiments require a sophisticated evaluation procedure of the measured data. In the case of absorption measurements, the measured quantity is the total absorption coefficient α. Absorption by free carriers, either measured or calculated using values for the free carrier density, the effective mass, and the mobility, has to be subtracted from the latter. Here, interconduction band transitions peaked at around 0.54 eV give rise to additional problems in extracting the absorption edge of the valence-to-conduction band transitions. α is then interpreted as consisting of a phonon contribution to indirect transitions and a part due to impurity or electron–electron scattering. The model for each contribution contains one unknown parameter. For the first contribution, this parameter is found by the measurements of the absorption in pure silicon and inserting a certain value for the phonon energy into the model (typically 50 meV). The second parameter together with the value of the indirect gap are adjusted for the best fit to the experimental data. Both models contain the Fermi level, which is commonly calculated with the ideal DOS. The crucial points in finding the gap in absorption experiments are the appropriate admixture of phonon-assisted transitions, the value of the phonon energy, and the extracted Fermi level. In PL experiments the knowledge of the true initial states (bound, exciton or band) is needed. The spectrum is blurred and weak in intensity. However, in PL measurements there is no overlap with intraband transitions. Furthermore, they allow a fairly unambiguous extraction of the Fermi level as compared to absorption measurements.

In Fig. 8 we compared our model with optical BGN measurements in n-type silicon (left part) and p-type silicon (right part), respectively. Data points are from Aw *et al.*[43] (transmission), Balkanski *et al.*[44] (transmission), Daub and Würfel[45] (PL), del Alamo *et al.*[46] (IR photoresponse of solar cells), Lanyon *et al.*[47] (IR photoresponse of transistor), Schmid[48] (transmission), Volf'son and Subashiev[49] (photo-

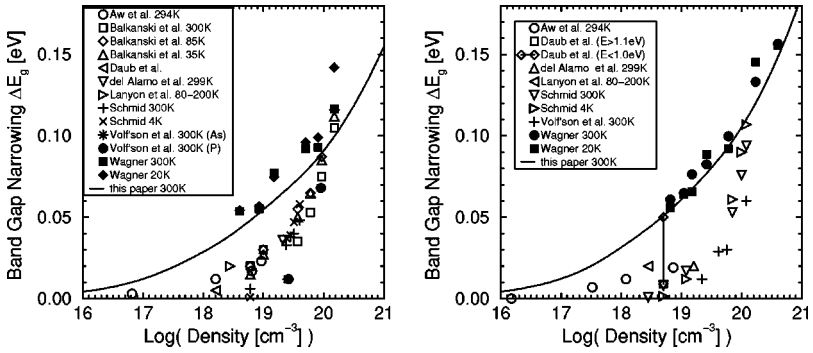

FIG. 8. Comparison with optical BGN measurements in n-type (left) and p-type (right) silicon, respectively.

conductivity), and Wagner[9] (PL). Our model shows a fairly good agreement with the PL data by Wagner, in particular for p-type silicon.

The electrical method is based on a measurement of the quantity $\mu_B n_i^2$ in a bipolar transistor and on the relation $\mu_B n_i^2 = I_C c_B/(A_E k_B T)$, where I_C is the collector saturation current, A_E the emitter area, c_B the total number of majority carriers per cm^2, respectively, and n_i^2 is replaced by the pn product in the base. The measured quantities are the collector current as function of the emitter-base voltage (from which I_C is derived), the sheet resistance underneath the emitter (from which c_B is found), and the minority carrier mobility μ_B in the base. The above formula only holds, if the device is 1D-like, homogeneously doped, if the depletion approximation can be applied, and if recombination in the base can be neglected. Since electrical data contain anything not considered in an analytical or numerical transistor model (including degeneracy effects), the term ''apparent'' BGN came into use.

Figure 9 shows the comparison with electrical (''apparent'') BGN data in n-type silicon as originally published (left part) and as revised by del Alamo and Swanson[6] with respect to mobility models and intrinsic density parameters (right part). Data points are from Abdurakhmanov *et al.*[50] (differential conductance of Si-Sn tunnel diodes), Mertens *et al.*[51] (dc measurements of n^+p diodes), Neugroschel *et al.*[52] (dc measurements of n^+p diodes and n^+pn transistors), Tang,[53] Wieder,[54] Wulms[55] (all from I_C in bipolar transistors), del Alamo and Swanson[6] (diffusion length, lifetime, and equilibrium density measurements in various npn transistor structures), and Possin *et al.*[56] (pn product in epitaxially grown bipolar transistors as a function of temperature). There is a remarkable agreement between the revised data points and our model in the density range 6×10^{18} to 1×10^{20} cm^{-3}. A distinct misfit exists around $n=10^{18}$ cm^{-3}, where the measured BGN almost vanishes.

Figure 10 shows the comparison with electrical (''apparent'') BGN data in p-type silicon as originally published (left part) and as revised by Klaassen *et al.*[1] in their ''unified apparent bandgap narrowing for n- and p-type silicon'' (right part). The original data points are from King and Swanson[57] (effective lifetimes in diffused emitters), Slotboom and de Graaff[2] (mobility and current gain in various npn transistors at various temperatures), Swirhun *et al.*[58] (diffusion length, minority carrier lifetime, and collector saturation current), and Tang[53] (collector current of bipolar transistor). Revised data for n- and p-type silicon include results from Klaassen *et al.*,[1] Ghannam,[59] Mertens *et al.*,[51] Neugroschel *et al.*,[52] Possin *et al.*,[56] Slotboom and de Graff,[2] Swirhun *et al.*,[58] and Wieder.[54] A good agreement between the revised experimental data and our model is observed for all densities.

Finally, we depict the carrier-impurity contribution to the band shifts in depletion regions in Fig. 11 as it turns out from the above discussed crude approximation. Also shown are the effective band shift due to the tail model of Van Mieghem *et al.*,[42] and the ΔE_g extracted from CV measurements on heavily doped diodes by Bennett and Lowney.[35,60,61] This ΔE_g was obtained by the difference be-

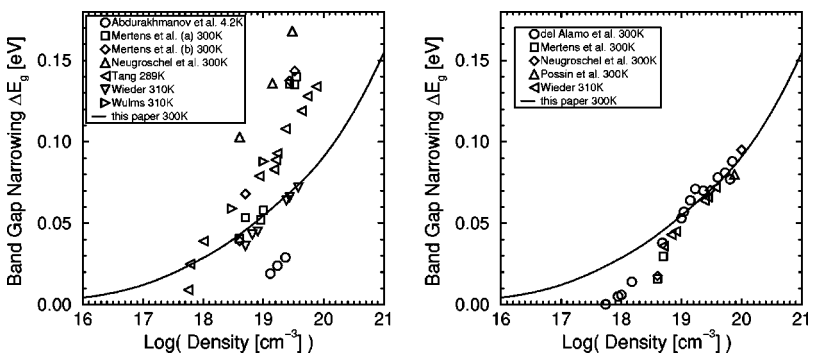

FIG. 9. Comparison with electrical (''apparent'') BGN data on n-type silicon. As originally published (left) and revised by del Alamo *et al.* (Ref. 6) (right), respectively.

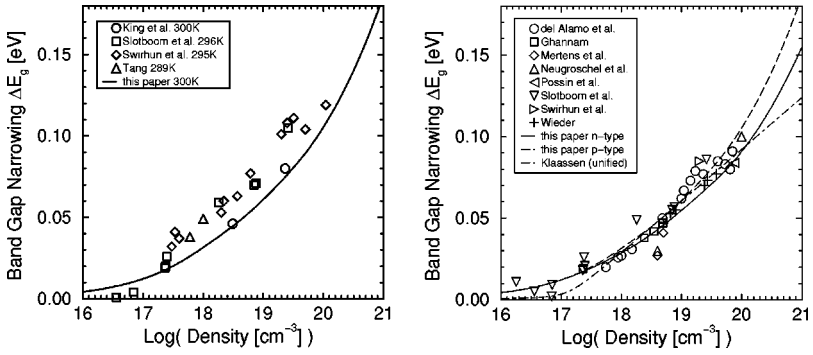

FIG. 10. Comparison with electrical (''apparent'') BGN data on p-type silicon. As originally published (left) and revised by Klaassen *et al.* (Ref. 1) (right), respectively.

tween theoretical and observed intercept voltage in a plot of the inverse capacitance cubed vs voltage.

C. BGN profiles in a bipolar transistor

Figure 12 demonstrates the application of the BGN model to a n^+pn transistor under increasing emitter-base voltage V_{BE}. All density profiles were obtained by a 1D cut through a 2D device simulated with the drift-diffusion mode of the device simulator DESSIS$_{-ISE}$.[62] In the depletion zone of the emitter-base junction there is a residual BGN of about 10 meV at zero bias, which forms a dip because of the relatively high base doping level. As the depletion region is flooded by carriers with rising V_{BE}, the BGN dip is washed out as a consequence of the increasing contribution of exchange-correlation to BGN. In contrast, heuristic models which only depend on the doping concentration, are independent of the injection conditions. For comparison, we included the profiles of the del Alamo model (n type[4]) and the Klaassen model (unified[63]). Two systematic failures are evident when applying heuristic models as function of only the doping: First, BGN is overestimated in depletion zones, since these models were derived from neutral regions. Secondly, using models for n- and p-type material simultaneously in compensated regions of a device will overestimate BGN, too. In the above example this would be the case in the emitter due to its relatively high acceptor level.

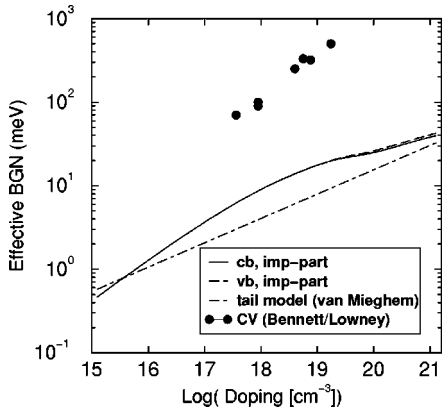

FIG. 11. Carrier-impurity contribution to the band shifts in depletion regions from the presented BGN model (solid and dashed lines), from the tail model of Van Mieghem *et al.* (Ref. 42) (dot-dashed line), and the ΔE_g extracted from CV measurements on heavily doped diodes by Bennett and Lowney (Refs. 35, 60, 61) (symbols).

V. CONCLUSIONS

We derived an analytical BGN model for silicon device simulation from a non-self-consistent finite-temperature full RPA calculation. The correlation energy of the carrier-dopant interaction was treated in the same manner as the exchange-correlation self-energy of the free carriers, assuming a random distribution of dopants on regular lattice sites. In order to prove whether the rigid shift approximation has a sound basis the dispersive exchange-correlation part of the QPS was numerically calculated in RPA quality in the density range $10^{17}-10^{20}$ cm^{-3} and for temperatures between 0 and 1000 K. The dispersion is flat for the relevant energies at all temperatures, and the sharp downward spike representative for the threshold of plasmon emission is quickly washed out as the temperature increases. The rigid shift approximation is consistent with the non-self-consistent RPA scheme. Conversely, if the dispersion is considered important, then also the QPS should be calculated self-consistently, which however is beyond todays computational means. Self-consistent results for $T=0$ have revealed a similar deviation between rigid and dispersive shift as between non-self-consistent and self-consistent approach, respectively. The flat dispersion is the result of a compensation of the strong individual dispersions of exchange part $\Delta^x(k)$ and correlation part $\Delta^c(k)$. A similar compensation effect leads to a pronounced temperature dependence of the BGN only in the intermediate concentration range around the Mott density. At room temperature, the $T=0$ limit becomes valid above densities of 10^{19} cm^{-3}. The contribution of the ionic part Δ^i of the QPS to the total BGN decreases from 1/3 at low densities to about 1/4 at very high densities. Strong screening makes Δ^i negligibly small under conditions of high injection.

Based on the numerical results for Δ^{xc} and Δ^i, Padé approximations in terms of carrier densities, doping, and temperature with an accuracy of 1 meV were constructed. For this, we used the limiting cases of high density/low temperature and low density/high temperature and the special cases of a symmetrical e-h plasma without doping and of doped, uncompensated silicon without excitation, respectively. In device application two major problems occur: spa-

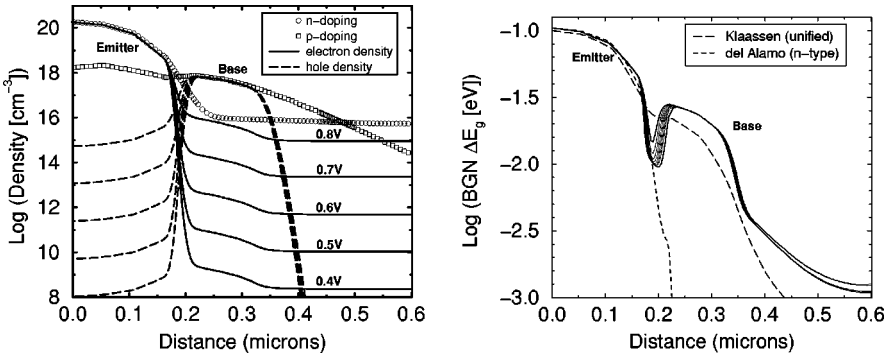

FIG. 12. Left: Doping and carrier density profiles in a n^+pn transistor under different injection conditions. The family parameter is the emitter-base voltage V_{BE}. Right: Corresponding band gap narrowing profiles using the model of this paper. The long-dashed curve represents the empirical model by del Alamo and Swanson (Ref. 6), the dashed curve the unified empirical model by Klaassen *et al.* (Ref. 1).

tial variations that are not slow compared with the correlation length, and SCRs. The former hampers the application to, e.g., a quasi-2D carrier gas in a MOSFET channel even when the confinement of states is disregarded. Depletion zones highlight the band bending in Δ^i and make its formal contribution to BGN divergent as a consequence of the huge screening radius in the dielectric function. An artificial cut of the screening radius, e.g., by the adjustment of an ''ion temperature'' (Stern[64]) was rejected, because the derivation of Δ^i was based on local charge neutrality and because the RPA fails for localized states in an unscreened dopant-carrier potential. Instead, a crude solution for device modeling was preferred, where the carrier densities in Δ^i were replaced by the respective concentrations of dopants. This leaves the result in neutral, uncompensated regions unchanged and gives an artificial rigid shift in SCRs which is comparable in size with the band tails caused by local potential fluctuations. Compared to experimental data, the device model shows a reasonable agreement with certain PL data and a good agreement with recently revised electrical measurements, in particular for *p*-type silicon. To demonstrate the dependence on carrier densities, BGN profiles in a bipolar transistor were simulated for increasing injection into the base. Significant differences to heuristic models which only depend on the doping are observed.

ACKNOWLEDGMENTS

The author is indebted to Dr. G. Heiser (UNSW Sydney) who implemented the model into the device simulator DESSIS$_{-ISE}$ and to Dr. P. Altermatt (UNSW Sydney) who allowed the author to use his complete BGN data collection. The author appreciates extremely valuable discussions with Professor R. Zimmermann (HU Berlin) and Dr. P. E. Selbmann (EPFL Lausanne).

[1] D. B. M. Klaassen and J. W. Slotboom and H. C. de Graaff, Solid-State Electron. **35**, 125 (1992).
[2] J. W. Slotboom and H. C. de Graaff, Solid-State Electron. **19**, 857 (1976).
[3] J. W. Slotboom and H. C. de Graaff, IEEE Trans. Electron Devices **24**, 1123 (1977).
[4] J. A. del Alamo, S. E. Swirhun, and R. M. Swanson, Solid-State Electron. **28**, 47 (1985).
[5] J. A. del Alamo and R. M. Swanson, IEEE Trans. Electron Devices **34**, 1580 (1987).
[6] J. A. del Alamo and R. M. Swanson, Solid-State Electron. **30**, 1127 (1987).
[7] H. S. Bennett and C. L. Wilson, J. Appl. Phys. **55**, 3582 (1984).
[8] J. Wagner, Phys. Rev. B **32**, 1323 (1985).
[9] J. Wagner, Solid-State Electron. **30**, 1117 (1987).
[10] J. Wagner and J. A. del Alamo, J. Appl. Phys. **63**, 425 (1988).
[11] S. M. Sze, *Physics of Semiconductor Devices*, 2nd ed. (Wiley, New York, 1981).
[12] A. Neugroschel, J. S. Wang, and F. A. Lindholm, IEEE Electron Device Lett. **6**, 253 (1985).
[13] E. K. Banghart and J. L. Gray, IEEE Trans. Electron Devices **39**, 1108 (1992).
[14] J. R. Lowney, J. Appl. Phys. **66**, 4279 (1989).
[15] M. Reaz Shaheed and C. M. Maziar, Solid-State Electron. **37**, 1589 (1994).
[16] G. D. Mahan, J. Appl. Phys. **51**, 2634 (1980).
[17] B. I. Lundqvist, Phys. Kondens. Mater. **6**, 193, 206 (1967).
[18] K.-F. Berggren and B. E. Sernelius, Phys. Rev. B **24**, 1971 (1981).
[19] K.-F. Berggren and B. E. Sernelius, Phys. Rev. B **29**, 5575 (1984).
[20] A. Selloni and S. T. Pantelides, Phys. Rev. Lett. **49**, 586 (1982).
[21] S. T. Pantelides, A. Selloni, and R. Car, Solid-State Electron. **28**, 17 (1985).
[22] R. A. Abram, G. N. Childs, and P. A. Saunderson, J. Phys. C **17**, 6105 (1984).
[23] L. Hedin and S. Lundqvist, Solid State Phys. **23**, 1 (1969).
[24] L. R. Logan and J. L. Egley, Phys. Rev. B **47**, 12532 (1993).
[25] R. Zimmermann, *Many Particle Theory of Highly Excited Semiconductors* (BSB Teubner Verlagsgesellschaft, Leipzig, 1988).
[26] M. Rösler, F. Thuselt, and R. Zimmermann, Phys. Status Solidi B **118**, 303 (1983).
[27] H. Stolz and R. Zimmermann, Phys. Status Solidi B **94**, 135 (1979).
[28] M. Rösler, R. Zimmermann, and W. Richert, Phys. Status Solidi B **121**, 609 (1984).
[29] R. Zimmermann and H. Stolz, Phys. Status Solidi B **131**, 151 (1985).
[30] P. Vashishta and R. K. Kalia, Phys. Rev. B **25**, 6492 (1982).
[31] F. Thuselt, Phys. Lett. A **94**, 93 (1993).
[32] M. Gell-Mann and K. A. Brueckner, Phys. Rev. **106**, 364 (1957).
[33] W. Ebeling, W. Richert, W. D. Kraeft, and W. Stolzmann, Phys. Status Solidi B **104**, 193 (1981).
[34] R. Zimmermann, E. H. Böttcher, N. Kirstaedter, and D. Bimberg, Superlattices Microstruct. **7**, 433 (1990).
[35] H. S. Bennett and J. R. Lowney, Solid-State Electron. **33**, 675 (1990).
[36] J. R. Lowney, J. Appl. Phys. **59**, 2048 (1986).
[37] G. L. Pearson and J. Bardeen, Phys. Rev. **75**, 865 (1949).
[38] P. P. Debye and E. M. Conwell, Phys. Rev. **93**, 693 (1954).
[39] J. R. Klauder, Ann. Phys. (N.Y.) **14**, 43 (1961).
[40] J. Serre and A. Ghazali, Phys. Rev. B **28**, 4704 (1983).
[41] E. O. Kane, Solid-State Electron. **28**, 3 (1985).
[42] P. Van Mieghem, S. Decoutere, G. Borghs, and R. Mertens, Solid-State Electron. **35**, 699 (1992).
[43] S. E. Aw, H. S. Tan, and C. K. Ong, J. Phys. C **3**, 8213 (1991).
[44] M. Balkanski, A. Aziza, and E. Amzallag, Phys. Status Solidi **31**, 323 (1969).
[45] E. Daub and P. Würfel, J. Appl. Phys. **80**, 5325 (1996).

[46] J. A. del Alamo, R. M. Swanson, and A. Lietoila, Solid-State Electron. **26**, 483 (1983).
[47] H. P. D. Lanyon, A. K. McCurdy, and R. A. Tuft, *Proceedings of the 13th IEEE Photovoltaic Specialist Conference, Washington D.C. 1978* (IEEE, New York, 1978), p. 60.
[48] P. E. Schmid, Phys. Rev. B **23**, 5531 (1981).
[49] A. A. Volf'son and V. K. Subashiev, Sov. Phys. Semicond. **1**, 327 (1967).
[50] K. P. Abdurakhmanov, S. Mirakhmedov, and A. T. Teshabaev, Sov. Phys. Semicond. **12**, 457 (1978).
[51] R. P. Mertens, J. L. van Meerbergen, J. F. Nijs, and R. J. van Overstraeten, IEEE Trans. Electron Devices **27**, 949 (1980).
[52] A. Neugroschel, S. C. Pao, and F. A. Lindholm, IEEE Trans. Electron Devices **29**, 894 (1982).
[53] D. D. Tang, IEEE Trans. Electron Devices **27**, 563 (1980).
[54] A. W. Wieder, IEEE Trans. Electron Devices **27**, 1402 (1980).
[55] H. E. J. Wulms, IEEE J. Solid-State Circuits **12**, 143 (1977).
[56] G. E. Possin, M. S. Adler, and B. J. Baliga, IEEE Trans. Electron Devices **31**, 3 (1984).
[57] R. R. King and R. M. Swanson, IEEE Trans. Electron Devices **38**, 1399 (1990).
[58] S. E. Swirhun, Y.-H. Kwark, and R. M. Swanson, Tech. Dig. Int. Electron Devices Meet. 24 (1986).
[59] M. Y. Ghannam, Ph.D. thesis, Katholieke Universiteit Leuven, 1992.
[60] J. R. Lowney, Solid-State Electron. **28**, 187 (1985).
[61] J. R. Lowney and W. R. Thurber, Electron. Lett. **20**, 143 (1984).
[62] DESSIS 3.0: Manual, ISE Integrated Systems Engineering AG, Zurich, Switzerland, 1996.
[63] D. B. M. Klaassen, J. W. Slotboom, and H. C. de Graaff, Solid-State Electron. **35**, 953 (1992).
[64] F. Stern, Phys. Rev. B **3**, 3559 (1971).